

Size-selective separation of magnetic nanospheres in a microfluidic channel

Jie Wu¹ · Qifan Yan¹ · Shouhu Xuan¹ · Xinglong Gong¹

Received: 18 January 2017 / Accepted: 21 February 2017
© Springer-Verlag Berlin Heidelberg 2017

Abstract This paper reported an efficient method to size-selective separate magnetic nanospheres using a self-focusing microfluidic channel equipped with a permanent magnet. Under external magnetic field, the magnetophoresis force exerted on particles leads to size-dependent deflections from their laminar flow paths and results in effective particles separation. By adjusting the distance between magnet and main path of channel, we obtained two monodisperse nanosphere samples (Ca. 90 nm, Ca. 160 nm) from polydispersing particles solution whose diameters varied from 40 to 280 nm. Based on the magnetostatic and laminar flow models, numerical simulations were also used to predict and optimize the nanospheres migrations. Two thresholds of particles diameters were obtained by the simulations and diverse at each position of magnet. Therefore, appropriate position of the magnet could be determined at a certain particle sizes' range when the flow rate of the two inlets remains unchanged.

Keywords Microfluidic channel · Magnetic nanospheres · Permanent magnet · Numerical simulations · Size-selective separate

1 Introduction

Due to the unique physical and chemical properties, magnetic nanospheres are appealing intense interest for

biomedical and bioanalytical applications from their bulk counterparts, for example as drug delivery vehicles (Bao et al. 2013; Singh and Sahoo 2014), photocatalytic materials (Song et al. 2015), cell sorting (Hejazian et al. 2015; Zhu et al. 2012) or plasmonic devices (Xi et al. 2015). Magnetic properties are significantly dependent on particles sizes when they come to nanometer range (Chatterjee et al. 2003). Especially, drug delivery systems require proper sizes of the Fe₃O₄ nanoparticles which affect nanoparticles clearance from circulation (Choi et al. 2007). For instance, medium-sized nanospheres (30–150 nm) have accumulated in the bone marrow, heart, kidney and stomach, while large nanospheres (150–300 nm) have been found in the liver and spleen (Veisoh et al. 2010). Obviously, the applications of the Fe₃O₄ nanospheres associated tightly with their sizes. To our knowledge, almost all the groups focused on the synthesis of magnetic nanospheres (Xuan et al. 2010; Figuerola et al. 2008), while only a few methods for producing pure and monodisperse nanospheres were reported. Therefore, it is centrally important to develop methods for sorting magnetic nanospheres whose diameters are within hundreds nanometers.

The magnetic field flow fractionation (MFFF) methods were the most commonly mentioned strategy to sort a range of magnetic materials including nano- and microparticles (Stephens et al. 2012). Jason et al. demonstrated an open tubular capillary column separation for different types of magnetic nanoparticles (Latham et al. 2005). A modified MFFF technique was designed by placing the separation channel in a quadrupole magnet (Carpino et al. 2007). Porous media were also used in the sorting and analysis of magnetic nanoparticles (Kim et al. 2009; Phan and Jones 2006). Munir et al. used tangential microfluidic channels and magnetic nanoparticles in magnetically actuated separation (Munir et al. 2014). Recently, microfluidic devices

✉ Xinglong Gong
gongxl@ustc.edu.cn

¹ CAS Key Laboratory of Mechanical Behavior and Design of Materials, Department of Modern Mechanics, University of Science and Technological of China, Hefei 230027, People's Republic of China

play an increasing important role in magnetophoretic particle sorting fields due to multiple advantages of microscale and magnetism effects, such as low reagent cost, comparatively fast reaction times, less invasiveness and noncontact (Vilkner et al. 2004; Whitesides 2006; Yavuz et al. 2006). Many groups performed intensive work in both experimental and numerical areas and presented various magnetic sorting methods with microfluidic devices during the last few years. Ferrofluids have been frequently employed for a variety of manipulations of diamagnetic or nonmagnetic particles in microfluidics for their large magnetic susceptibility (Hejazian and Nguyen 2015; Zhu et al. 2010, 2011). Most cells are inherently diamagnetic and mismatch magnetic susceptibility to ferrofluids; thus, the repulsive force generated by an externally applied magnetic field gradient was used to move labeled free cells away from the magnetic source (Rodriguez-Villarreal et al. 2011; Shen et al. 2012; Zeng et al. 2012). Kwang et al. presented a droplet-based microfluidic platform to sort magnetic particle for magnetic bead-based bioassays (Lee et al. 2012). In addition, numerical simulations were also proposed by several researchers to obtain the particle trajectories in magnetic sorting. Xuan et al. simulated the diamagnetic and magnetic particles trapping in ferrofluids' flow simultaneously (Zhou et al. 2015). Li, Cheng introduced a three-dimensional analysis of magnetic sorting in 2014 (Han et al. 2014; Cheng et al. 2014). Recently, magnetoconvective drag force on the magnetic stream was also introduced to analyze the dominant force involved in the manipulation of particles in microfluidics (Hejazian and Nguyen 2016; Hejazian et al. 2016). A finite element mathematical model was successfully developed for demonstrating an innovative time-dependent magnetically actuated mixing process (Munir et al. 2009a, b, 2010, 2011).

However, current magnetic sorting studies were mainly focused on microscale particle. For microfluidic system, only a mathematical model based on finite element technique has been developed to predict the migration and capture of multiple magnetic nanoparticles (Munir et al. 2009a, b). Few work responded for the experimental processes was reported till now, which further obstructed the popularization of this model. In consideration of the important application of the monodisperse magnetic nanospheres, developing a feasible method to purify magnetic nanospheres in microfluidic devices is urgently needed. In this work, based on the microfluidic device equipped with a permanent magnet, a convenient size-selective separation approach to sort magnetic nanospheres was reported. We focused nanospheres into a tight stream with the help of self-focusing channel design and high flow rate ratio of two inlets. It was an essential step in the manipulations. Then, numerical simulations were proposed to obtain the nanospheres trajectories. The magnetic field and its gradient

played crucial roles in nanospheres migrations. Two thresholds of particles diameters were obtained in each situation. TEM images and dynamic light scattering results of obtained nanospheres demonstrated the validity of this experiment. It was found that the experimental data were consistent with the numerical simulations.

2 Experiment

2.1 Device fabrication

The polydimethylsiloxane (PDMS) device was fabricated through a standard soft-lithography technique (Duffy et al. 1998). At first, the layout of the device was designed by CorelDRAW and printed on a film as the photomask in the photolithography process. The negative photoresistor (SU-8-2075, MicroChem) was coated on a Si wafer and then placed on a spin coater to create molds. The spin coating processing was set at 1000 rpm for 18 s and 3000 rpm for 1 min to make the 50–70 μm thickness, which equaled to the rectangular channel depth. The obtained dry photomask film was placed upon the Si wafer resisting exposure of the photoresistor lamination out of the channel. Then, PDMS (Sylgard 184, Dow Corning) mixture (10 A: 1 B) was poured onto the master mold. After the degassing in a vacuum desiccator for 5 min, it was cured in an oven at 90 $^{\circ}\text{C}$ for 20 min. The solidified PDMS was peeled from the Si wafer and rinsed by ethanol for 5 min. Finally, the rinsed PDMS and glass slide were dried in an oven at 80 $^{\circ}\text{C}$ and treated by a plasma cleaner (PDC-36G, MTI Corp.) for 30 s. The PDMS and glass slide were bonded immediately, and then the microfluidic chip was obtained.

Figure 1 shows the schematic and dimensions of the device used in the experiments. Figure 1a shows a photographic image of the microfluidic chip. The device had 15 mm length and 0.2 mm width of the main flow path (Fig. 1b). Figure 1c and d shows the details of the two inlets and two outlets. The sample was injected into the channel through inlet 1, which was 50 μm in width. At the same time, buffer solution (deionized water) was injected into the channel through 150 μm width inlet 2. The corresponding two outlets were both 100 μm in width for collection of the deflected target nanospheres.

2.2 Synthesis of magnetic nanospheres

Magnetic Fe_3O_4 nanospheres were synthesized in a binary solvent system with diethylene glycol (DEG) and ethylene glycol (EG) (Xuan et al. 2010). Briefly, $\text{FeCl}_3 \cdot 6\text{H}_2\text{O}$ (2.16 g), NaAC (8 g) and PAA (0.2 g) were dissolved in an 80 mL mixture of DEG (60 mL) and EG (20 mL). After magnetic stirring for 30 min, the obtained yellow solution

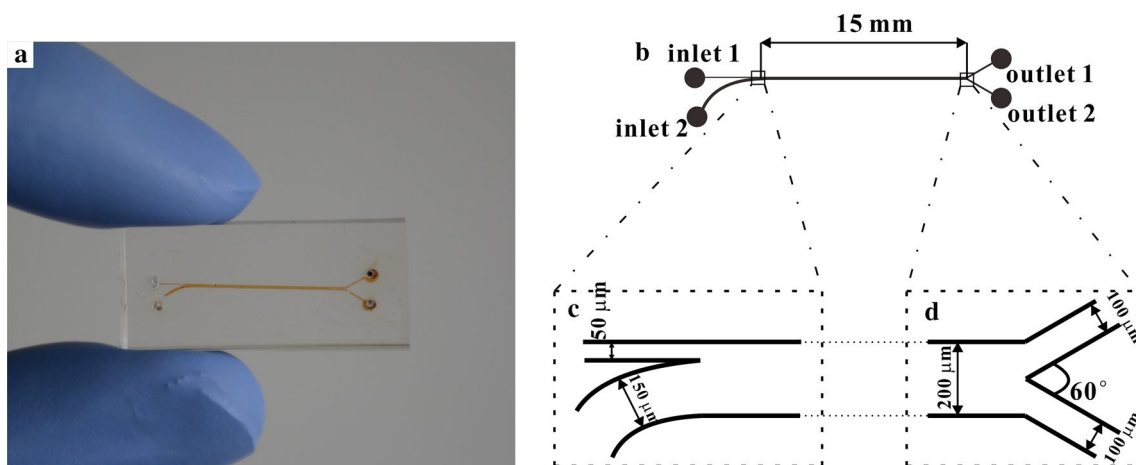


Fig. 1 **a** A photographic image of prototype device. **b** Schematic of the device. It contained 15 cm length, 0.2 mm width main path, two inlets and two outlets. Specific figures of **c** inlets and **d** outlets. The widths of two inlets and two outlets were 50, 150, 100 and 100 μm , respectively

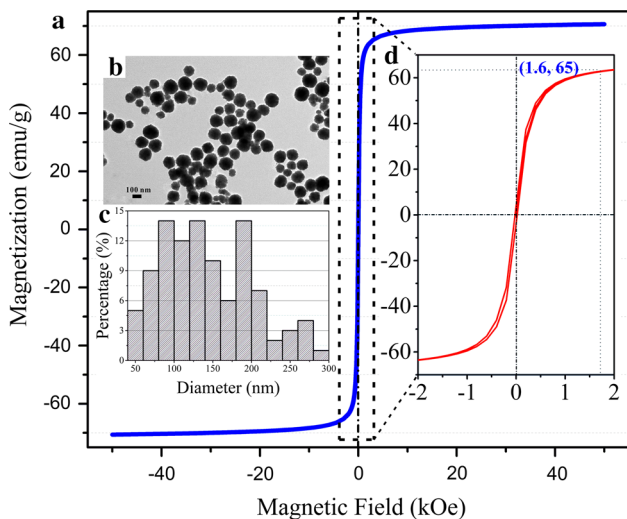


Fig. 2 **a** Magnetic hysteresis loop (magnetization versus an applied magnetic field) of Fe_3O_4 nanospheres. **b** TEM image of initial Fe_3O_4 nanospheres obtained by using the binary solvent system. **c** Histograms of particle sizes' distribution of the initial Fe_3O_4 nanospheres. **d** Enlarged drawing at low magnetic field strength. Coordinate showed their saturation magnetization and corresponding magnetic field strength

was transferred into a Teflon-lined stainless-steel autoclave. The sealed reactor was heated at 200 °C for 720 min. By cooling to room temperature, the obtained Fe_3O_4 nanospheres were washed by ethanol and deionized water for five times, respectively. Finally, about 0.6 g Fe_3O_4 nanospheres were achieved under drying in a vacuum oven. TEM image and the histogram of their particle size distribution showed that these particles had a broad particle size distribution (inset Fig. 2b, c). They denoted that Fe_3O_4 nanosphere diameters were varied from 40 nm to 280 nm, approximately. Then, the Fe_3O_4 nanospheres were

dispersed into water to form a uniform magnetic fluid for further purification.

The magnetic properties of the Fe_3O_4 nanospheres were investigated by a MPMS VSM (SQUID, Quantum Design Co., America) at room temperature. When the magnetic field strength reached to 1.6 KOe, the Fe_3O_4 nanospheres reached to saturation magnetization, 65 emu/g (inset Fig. 2d). Taking into account the entire test time, the design step in this experiment was set as 100 Oe, which indicates the superparamagnetic behavior. The hysteresis loop was smooth, and no obvious hysteresis was found indicating the coercive force and the residual magnetization approach to zero. Actually, these Fe_3O_4 nanospheres are composed of large amount of nanograins, thus revealing the cluster-like nanostructure. This phenomenon has been reported in many literatures (Fang et al. 2011; Liu et al. 2011). Because the average size of the nanograins was smaller than 16 nm, the final nanospheres exhibit superparamagnetic characteristics.

2.3 Experimental setup and procedure

Microfluidic channel system, magnetic field and observation system constituted the experimental setup (Fig. 3a). The channel was placed on the working stage of an inverted microscope. There were two inlets and two outlets (Fig. 1), and four polyethylene tubes (Smiths medical, 0.38 mm ID, 1.09 mm OD) were inserted into the holes of the device. Two highly accurate syringe pumps (LSP02-1B, Longer-Pump) connecting to the tubes were used to pump the sample and buffer solution into the channel through inlet 1 and inlet 2, whose flow rates were kept at 0.01, 0.04 mL/h, respectively. Magnetic field in microfluidic channel was provided by a permanent neodymium iron boron (NdFeB)

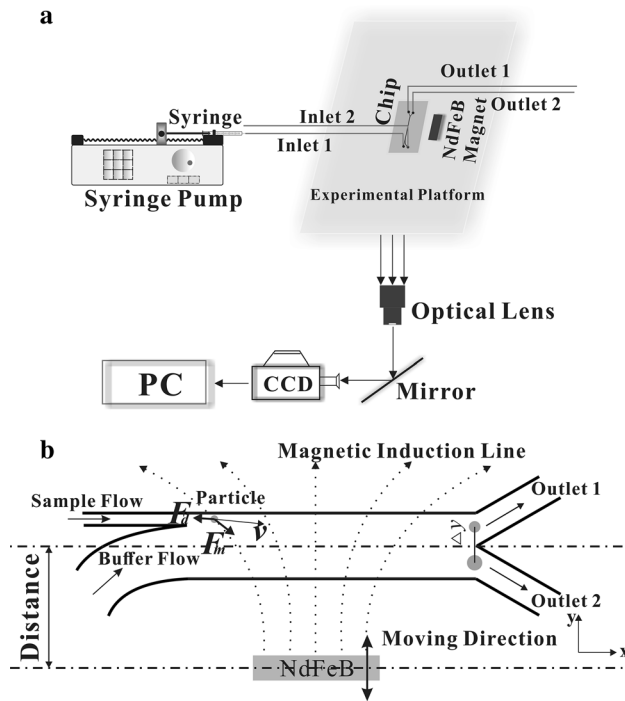


Fig. 3 a Schematic illustration of the proposed experimental setup. b A detailed view of the sorting device. The nanospheres were attracted by magnetic force to deflect toward the permanent magnet, and the trajectory exhibits the particle size dependency

magnet that was $10 \times 2 \times 5\text{mm}^3$ in size and the remnant field strength $B_r = 1.2\text{ T}$. The magnetic field strength over the channel area was tunable by changing the perpendicular distance between magnet and device. While the sample and buffer solution were being pumped and injected into the channel, the images of trajectory of the nanosphere were captured via the microscopy and a CCD camera (Nikon, Japan).

Due to the low Reynolds number of the microfluidic flow, there is a distinct interface between the sample and the buffer solution in the channel when the permanent magnet placed parallel to the main path is located far away from the channel or when the magnet is absent. Moving the magnet toward channel in the direction of the arrow shown in Fig. 3b, the magnetic nanospheres dispersed in the fluid were deflected to the buffer solution at the same time. Then, the fluid color would be gradual changed in the channel and the interface would disappear eventually. The distance between main path and magnet, exhibited in Fig. 3b, is one of the most important parameter in this experiment. Different suitable distances correspond to different size distribution. Therefore, numerical simulations are necessary to analyze particles migrations and give appropriate distance when the flow rate of the two inlets is kept constantly.

3 Theory and simulation

3.1 Force and analysis

A microfluidic channel equipment with a permanent magnet consisted in the system. Typically, the magnetic nanospheres' motion in the fluid and buffer solution under external magnetic field was governed by various forces and interaction including Stokes drag force, magnetic force, gravity and buoyance force. Because of the low Reynolds number in a microfluidic channel (Groisman and Quake 2004), inertial effect on the nanospheres was negligible and then the trajectories can be confirmed by considering dominant Stokes drag force and magnetic force. It's worth mentioning that magnetoconvective drag force on the magnetic stream is another force involved in particle manipulation (Hejazian and Nguyen 2016; Hejazian et al. 2016). Magnetic field induced bulk force caused magnetoconvective flow on paramagnetic fluid. As the magnetic particles used here were only Fe_3O_4 in the sample and they were far away from the magnet poles, the effect of magnetoconvective drag force was ignored in our work.

Magnetic force Exposed to magnetic field, a magnetized body dispersed in fluid experiences magnetic force, F_m , which can be generally expressed as Eq. (1) (Gijs et al. 2009; Tzirtzilakis 2005).

$$F_m = \iint \left(\frac{1}{2} \mu_0 M_n^2 + \mu_0 \int_0^H M dH \right) ndS \quad (1)$$

Here, S is the surface area of the nanosphere, and H is magnetic field strength. Permeability of vacuum $\mu_0 = 4\pi \times 10^{-7} \text{N} \cdot \text{A}^{-2}$. M_n means normal component of ferrofluid magnetization adjacent to the surface S enclosing the particle. As a result, the magnetic force can be simplified to.

$$F_m = \mu_0 V (\mathbf{M} \cdot \nabla) \mathbf{H} \quad (2)$$

where V is the volume of the magnetic nanosphere, \mathbf{M} is the vector of magnetization, and \mathbf{H} is the magnetic field strength at the center of the particle (Hejazian and Nguyen 2015).

As the weak magnetic field strength generated by a permanent magnet (Figs. 4 and 5 proved that the magnetic field was about 0.4–0.8 KOe ($\mathbf{H} = \frac{\mathbf{B}}{\mu_0}$) in the microfluidic channel.), the magnetization of the nanosphere depends approximately linearly on the applied magnetic field strength, which means $\mathbf{M} = \chi_p \mathbf{H}$, where χ_p is the susceptibility of the particle. Therefore, Eq. (2) can be translated to Eq. (3).

$$F_m = \mu_0 \chi_p V (\mathbf{H} \cdot \nabla) \mathbf{H} \quad (3)$$

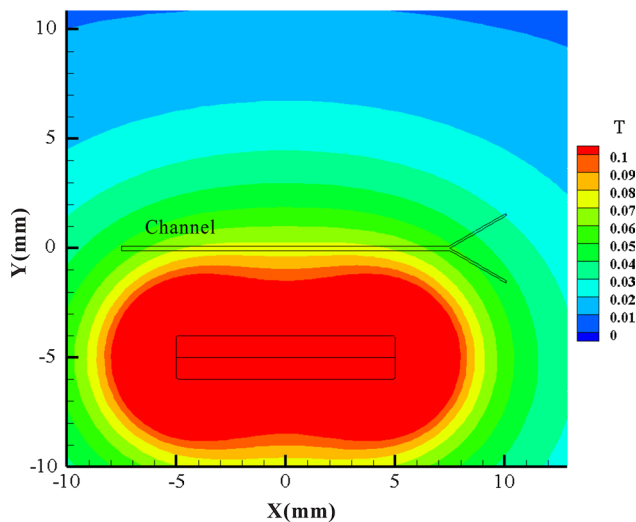


Fig. 4 Magnetic field density of the microfluidic channel

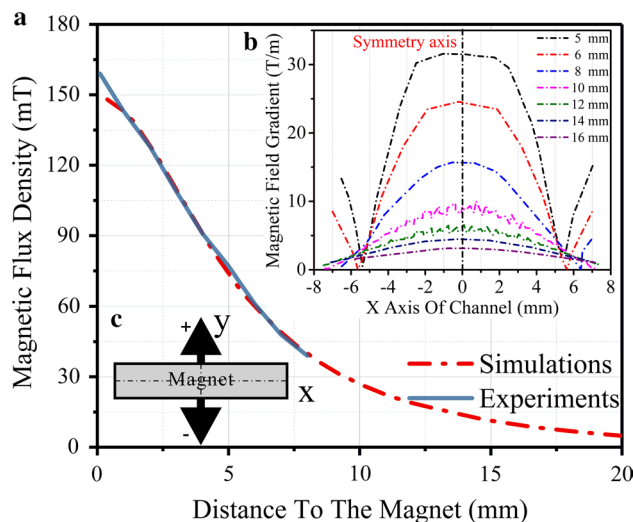


Fig. 5 a Magnetic flux density along positive direction of y-axis of the magnet. Red dash dot line for simulations results. Blue solid line for experimental data measured by a Teslameter. b Magnetic field gradient versus x-axis of channel at different distance. The black axes meant symmetry axis of the channel. c Coordinate axis of magnet (inset in figure) (color figure online)

Stokes drag force There is a resistance from the surrounding fluid named hydrodynamic drag force when a nanosphere moves. Reynolds number is very small and much less than 1 in a typical microfluidic channel, and the force caused by the viscosity of medium can be expressed as Eq. (4) (Iiguni et al. 2004).

$$F_d = 3\pi\eta D(\mathbf{v}_f - \mathbf{v}_p)f_D \tag{4}$$

where η is viscosity of surrounding fluid, D is diameter of nanosphere, and \mathbf{v}_f and \mathbf{v}_p are velocity vectors of

surrounding fluid and the nanosphere dispersed in it. f_D is hydrodynamic drag force coefficient of the particle, which accounts for the increased resistance where the particle closes to the microfluidic channel surface (Gijs et al. 2009). It has a form of

$$f_D = \left[1 - \frac{9}{16} \left(\frac{D}{D + 2z_p} \right) + \frac{1}{8} \left(\frac{D}{D + 2z_p} \right)^3 - \frac{45}{256} \left(\frac{D}{D + 2z_p} \right)^4 - \frac{1}{16} \left(\frac{D}{D + 2z_p} \right)^5 \right]^{-1} \tag{5}$$

where z_p is the distance between channel wall and particle's surface.

Velocity profile in the main path Particles are generally thought to follow fluid streamlines under laminar flow conditions, when no external forces are applied. The deflecting velocity caused by magnetic field is a crucial parameter determining the efficiency of separation of nanospheres. In this low Reynolds number microfluidic flow, inertial part of the kinematic equation is negligible because of the tiny mass of nanosphere. Finally, the balance equation can be simplified as.

$$F_d + F_m = 0 \tag{6}$$

After substituting (6) into (3) and (4), the velocity can be inferred as.

$$v_p = \frac{F_m}{3\pi\eta D f_D} \tag{7}$$

3.2 Numerical simulations

Considering the dominant magnetic force and Stokes drag force, COMSOL 4.4 (COMSOL Inc., USA), a finite element software package, was used to establish the numerical model to predict and optimize the trajectories of nanospheres. This model consisted of three application modes. A permanent Neodymium magnet, microfluidic channel and its surrounding PDMS constituted the three distinct domains.

The trajectories of nanospheres in the microfluidic channel were obtained through two separate steps. First, these two application modes, "magnetic fields, no currents" and "creeping flow," calculated magnetostatic and laminar flow models in a static way.

In a current-free region, the magnetic field is described using Maxwell–Ampere's law, where

$$\nabla \times \mathbf{H} = 0 \tag{8}$$

\mathbf{H} is the magnetic field strength. It is possible to define the scalar magnetic potential, V_m , from the relation

$$\mathbf{H} = -\nabla V_m \tag{9}$$

Constitutive relation is used in this mode to describe a relation between magnetic flux density \mathbf{B} and magnetic field strength \mathbf{H} by following equation

$$\mathbf{B} = \mu(\mathbf{H} + \mathbf{M}) \quad (10)$$

Here, $\mu = \mu_0\mu_r$ is the magnetic permeability where μ_r means relative permeability, and \mathbf{M} is the magnetization. Together with Gauss law for magnetic flux density, there is

$$\nabla \cdot \mathbf{B} = 0 \quad (11)$$

Then, we can derive an equation for V_m ,

$$-\nabla \cdot (\mu \nabla V_m - \mu \mathbf{M}) = 0 \quad (12)$$

A mathematical mode, Coefficient Form PDE, was used to calculate the gradient of the magnetic field strength. The results of pervious mode were used as the initial values. Functions (10) and (12) are used to calculate the magnetic field in the simulations.

The creeping flow application was used for simulating fluid flow at very low Reynolds number. In this case, the inertial term in Navier–Stokes equations can be neglected. It is assumed that the Fe_3O_4 magnetic nanospheres with a particle size distribution in the range of 40–280 nm were homogeneously dispersed in deionized water. Their viscosity and density were set equal to that of water because of the low mass fraction of the sample. No slip condition was applied along the walls of microfluidic channel and the two outlets, and pressure condition was set equal to zero and suppresses backflow.

The governing Navier–Stokes equation including the flow rate \mathbf{v} is described as

$$\rho \mathbf{v} \cdot \nabla \mathbf{v} = \mathbf{f}_b - \nabla p + \eta \nabla^2 \mathbf{v} \quad (13)$$

And there is

$$\rho \nabla \cdot \mathbf{v} = 0 \quad (14)$$

for this incompressible fluid. Here, p is the pressure, η is the viscosity of the fluid, and \mathbf{f}_b means the volume force acting on the particle. These two functions were used to calculate the application mode of creeping flow.

The influence of diffusion was neglected in the article. In order to effectively separate these particles, the forces (magnetic force and hydrodynamics force with Brownian force) must exceed the typical Brownian force $F_B = \zeta \sqrt{\frac{6\pi k_B T d_p}{\Delta t}}$, where T is temperature, k_B is Boltzmann's constant, d_p is diameter of Fe_3O_4 nanospheres, and Δt is the magnitude of the characteristic time step. The threshold diameter for Fe_3O_4 particles in water is $d_p = k_B T / |F| = 40\text{nm}$, where $|F|$ is the magnitude of the total force acting on the particle (Furlani 2006). For the tiny particles in the sample, forces may be in the similar scale, and diffusion affected the effect of separation.

However, the sample flow containing these tiny particles was on the side of the main path of the channel remote from the magnet. Since the magnetic field was weak, the diffusion due to the Brownian motion didn't cause the tiny particles to flow out through the outlet 2 as the extremely short time. The whole time for the sample to flow through the entire channel was approximately to 1 s. As a result, there was no adverse effect on the experimental purpose. So we neglected the effect of diffusion in simulations. In addition, this also saves computation time.

Then, particle tracing for fluid flow was used to trace the particles' trajectories with a time-dependent solver based on the results from the first two application modes. Here, drag force and magnetic force were the two main forces, which were calculated based on the above two mode, and were considered in this mode. Function 7 gave the velocity of movement of the particles in the microchannel. The wall condition here was set as freeze. Initial position was uniform distribution, and number of particles per release was 80.

Because the magnetic fields and creeping flow have different demands in meshing quality and computational domains, different computational grid size was used for solving these two application modes.

For the magnetic fields, we didn't have to manually mesh because of relatively low demands of meshing quality in microscale. The sequence type was set as physics-controlled mesh, and element size was set as extremely fine. As a result, the number of degrees of freedom was 156,994 in the simulation. On the other hand, we subdivided the grid and made smooth transition at the inlet and outlet of the channel to improve calculation accuracy for creeping flow. We found that the independence of the solution for the mesh size is achieved with a size of 2 μm , where the decrease in the mesh size has little effect on the numerical result. The number of elements was 48,552, and triangular element was used.

4 Results and discussion

4.1 Magnetic field and forces mapping

The first aim of the simulations was to evaluate the magnetic field properties of a centimeter-sized NdFeB permanent. Commercial finite element software was performed in 2D geometries (Figs. 4 and 5), to characterize the magnetic flux density and magnetic field gradient.

The simulations shown in Fig. 4 indicated that the value of magnetic flux density in the microfluidic channel was between 40 and 80 mT, where the distance (Fig. 3b) between magnet and main path of channel was 5 mm.

In this experiment, the nonuniform magnetic field exerted on the system using a permanent magnet at variable distance from 2 to 20 mm. In order to study the magnetic force acting on the particles, magnetic field gradient was another crucial data in the manipulations. The simulation results are summarized in Fig. 5. According to Eq. (3), the product of magnetic flux density and magnetic field gradient was proportional to magnetic force. Figure 5a presents the magnetic flux density value of the central position of microfluidic channel versus the distance to the permanent magnet. The maximum value was evaluated to be 150 mT when the magnet was nearby the channel and decreased to nearly zero once the distance reached 20 mm. The magnetic flux density was also measured by a Teslometer. The measured values in Fig. 5a were almost consistent with the results of numerical simulations. The magnetic field gradient of the main path ($-7.5 \text{ mm} < x < 7.5 \text{ mm}$) was calculated by the simulations at different distance (Fig. 5b). There was a distinct value terrace of magnetic field gradient with tiny fluctuation when the distance was less than 12 mm. In addition, the length of the terrace decreased quickly as the distance increased. For the sake of symmetry, these inflection points appeared in the horizontal axis

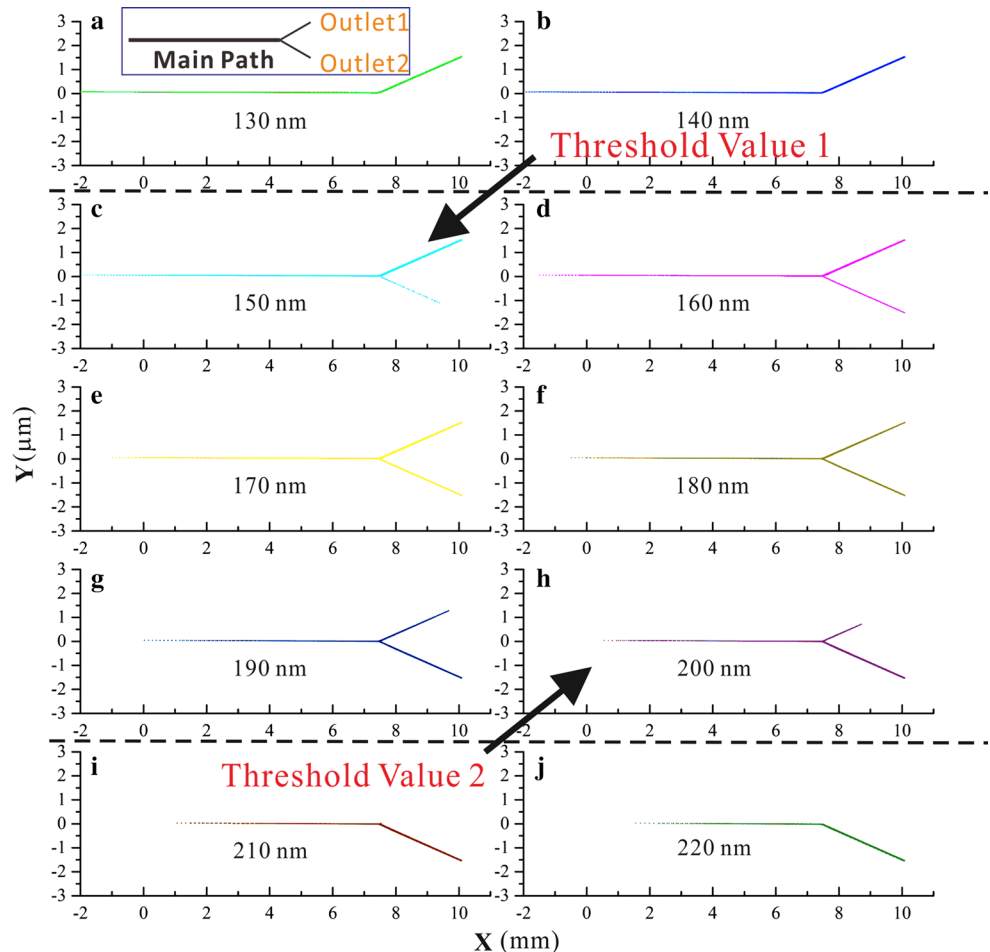
of $\pm 5.5 \text{ mm}$, which happened to be the edge of the magnet. The magnetic field gradient decreased from the central position to the two edges of the channel except for the much close distance. There was a slight increment in magnetic field gradient near the edges at these situations that showed the complicated condition in the surrounding area of the magnet. The distance between magnet and main path is first depicted in Fig. 3b. The x -axis and y -axis are shown in insets of Fig. 5c.

4.2 Particles trajectories

In this section, the simulations were firstly carried out with different Fe_3O_4 nanosphere sizes (130–220 nm) to observe the particles' trajectories in the microfluidic devices. The extent of magnetic deflections depended mainly on the balance between magnetophoresis force and hydrodynamic drag force. The inlet flow rate of the two inlets was both set as 14 mm/s since the volume flow rate of two syringe pumps was 0.05 mL/h in total.

Figure 6 shows the results of the simulations when distance between magnet and main path of channel was set as 5 mm. As shown in these trajectories, the deflections

Fig. 6 Fe_3O_4 nanosphere trajectories in microfluidic channels with different diameter sizes from 130 to 220 nm, **a** 130 nm, **b** 140 nm, **c** 150 nm, **d** 160 nm, **e** 170 nm, **f** 180 nm, **g** 190 nm, **h** 200 nm, **i** 210 nm, **j** 220 nm. **a, b** Outlet 1 was the only exit. **c–h** Outlet 1 and outlet 2 were both exits. **i, j** Outlet 2 was the only exit. Outlet 1 and outlet 2 are first mentioned in Fig. 1a. Schematic of the channel (inset in Fig. 6a). The two arrows in the figure presented the transition state of particles outlets. The permanent magnet was placed 5 mm away from the channel at these simulations



for different sizes nanospheres were diverse from 130 to 220 nm. Figure 6 is divided into three parts to analyze the particles trajectories. Figure 6a, b indicates all of the particles whose diameters were not exceeding 140 nm couldn't be attracted to the outlet 2 near the magnet. Besides, it was concluded that these particles whose diameters between 150 and 200 nm were partly attracted to outlet 1 and partly attracted to outlet 2. Comparing Fig. 6c and h, more and more particles flowed out of the outlet 2 with the increasing of particles diameters. Furthermore, the outlet 2 was the only exit to these nanospheres whose diameters reached 210 nm are shown in Fig. 6i and j. Schematic of the device is shown as an inset in Fig. 6a. As a consequence, 140 and 210 nm were two thresholds of particles diameters in the particle sorting.

The polydispersed magnetic fluids in this experiment had a broad diameters distribution ranging from 40 to 280 nm (Fig. 2b, c). Figure 7 describes the trajectories of polydisperse nanospheres in the microfluidic channel. The magnetic particles having a size in the range of 110–220 nm were attracted to the direction of magnet and flowed out from outlet 1 or 2, depending on the particles diameters in these situations. The deflection curves of these

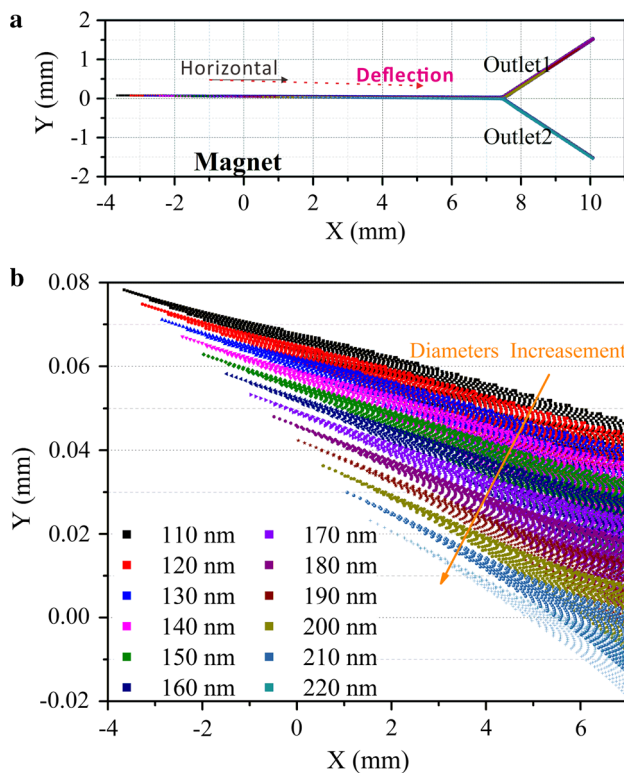


Fig. 7 **a** Trajectories of polydisperse nanospheres (110–220 nm) in a microfluidic channel. A weak deflection of these particles was exhibited by the red dotted arrow. **b** Enlarged details of trajectories in the main path of microfluidic channel. The orange arrow meant the direction of diameters increment (color figure online)

particles are shown in Fig. 7a. Further, an enlarged view, Fig. 7b, was used to depict trajectories of nanospheres with different diameters. There were distinct flow layers of each size particles, and the particles with larger diameter showed larger deflection of the trajectories in the channel. The orange arrow in Fig. 7b indicated the direction in which the particles diameters increased. The results of all these simulations were obtained at a constant flow rate, and the magnet was placed in the same position.

The effect of the permanent magnet position was also considered. To sort magnetic nanospheres in a microfluidic channel, we moved the permanent magnet perpendicularly to the main path of the channel. The moving direction is shown in Fig. 3b. Here, we introduced the concept of thresholds in order to illustrate the relationship between particle diameters and the corresponding channel outlets. Figure 6 shows that when the particles' diameters were less than or greater than a certain value, outlet 1 or outlet 2 could be the only exit of the nanospheres in the microfluidic channel and this value was called threshold. It was just in this condition to show excellent size-selective separation performance. Therefore, thresholds of particles diameters played a crucial role and were diverse at each distance in a constant inlet flow rate. The results of numerical simulations indicated the thresholds of nanospheres diameters at different positions of magnet (Fig. 8). Both two thresholds of particles diameters grew as the distance grew from 4.0 to 6.0 mm. The thresholds of nanospheres had a relatively rapid increment, since the magnetic field was drastically smaller as the distance increase. It was concluded that the diameters of nanospheres in magnetic fluid would

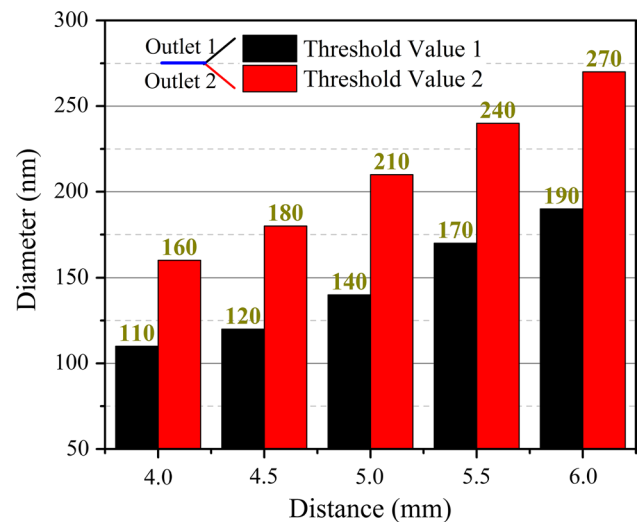


Fig. 8 Two thresholds of particle diameters versus the distance between magnet and main path of channel. The distance was increased from 4 to 6 mm with step size of 0.5 mm in the simulations. The two inlet flow rates were both set as a constant of 14 mm/s

correspond to different suitable distances of magnet to main path in different ranges.

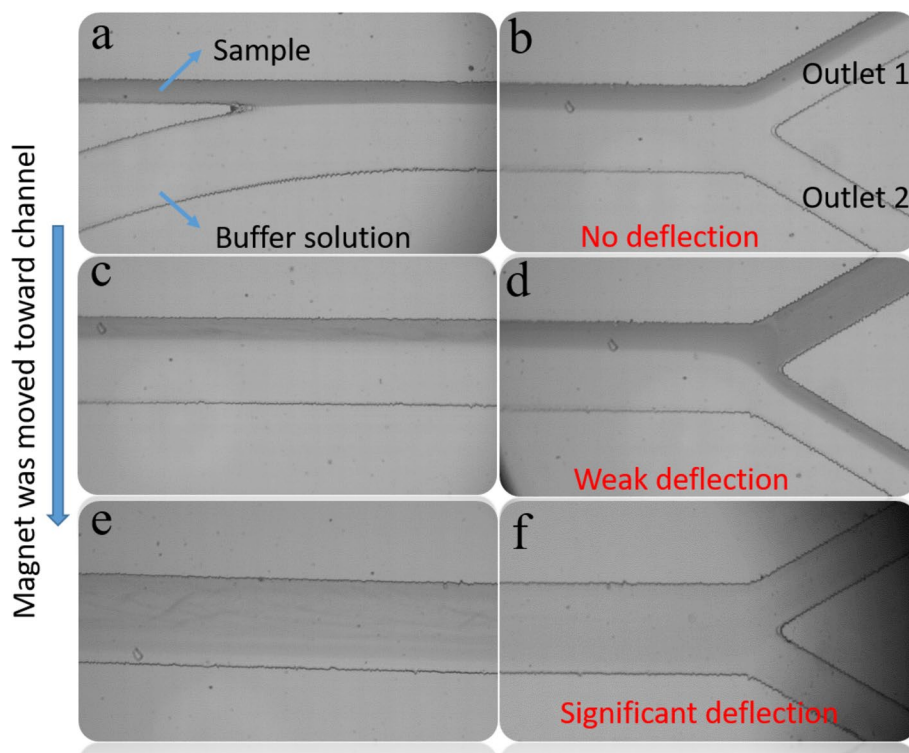
4.3 Experimental results and comparison

The obtained Fe_3O_4 nanospheres synthesized by the solvent–thermal method were dispersed in deionized water to form mother magnetic fluid with mass fraction of 5 wt%. Because there is large amount of polyacrylic acid exist on surface of the Fe_3O_4 nanospheres, the Fe_3O_4 nanospheres can be well dispersed within the water without large aggregation. Moreover, these Fe_3O_4 nanospheres are superparamagnetic; thus, few dipole–dipole interactions exist without applying the magnetic field. Furthermore, the low fraction also leads to a large distance between the Fe_3O_4 nanospheres, which further reduce the particle aggregation. Then, the mother fluid was injected into the channel by a highly accurate syringe pump through inlet 1, and buffer solution was injected into the channel through inlet 2 at the same time by another syringe pump. Since the much low Reynolds number of microfluidic flow, there was a distinct interface (Fig. 9a) between the mother fluid and buffer solution. The permanent magnet was placed far away from the main path of the device at this situation. The magnetic fluid flowed along their own focused width and maintained their flow path. Figure 9b denotes that outlet 1 was the only exit for all of the samples in this situation. Typically, when the permanent magnet was moved toward the channel, the

flow path of the magnetic fluid was shifted. Clearly, the deflection of flow path increased with the distance between magnet and main path decreased (Fig. 9c, e). Because of the increase in magnetic field strength and magnetic field gradient, the magnetic nanospheres dispersed in the fluid were deflected into the buffer solution, which led to the color gradient in width direction of the microfluidic channel. The relatively large particles in the fluid would be deflected significantly because of the large magnetic forces. Due to the precision limit of the optical microscope, the trajectory of an individual nanosphere in the channel couldn't be depicted by these photographic pictures. In contrast of Fig. 9b, d and f, it was found that more and more particles flow out the channel through outlet 2 while the magnet was being moved toward the channel. Therefore, these relatively large nanospheres would be separated from the initial fluid, and the aim of sorting has been completed as well. By the way, the condition revealed by Fig. 9e and f was an ideal situation for separating, and the corresponding distance between magnet and channel was a suitable position for sorting manipulation. The distance between the magnets to the channel structure can be dynamically controlled. In the further work, a computer controlling magnet will be used to exactly tuning the distance during the experiments.

Here, the polydisperse Fe_3O_4 nanosphere fluids with a broad size distribution were injected into the microfluidic device. After the sorting process, the fluids flowed out through outlet 1 and outlet 2 were collected, respectively.

Fig. 9 Photographic pictures of microfluidic channel. Magnetic nanospheres dispersed in deionized water were attracted toward the permanent magnet under the effect of the applied magnetic field. **a** The inlet area of channel. **b, d, f** The outlet area of channel. **c, e** The main path area of channel. *Gray areas* in the figures meant deionized water dispersing magnetic nanospheres, and *dark gray* and *light gray* denoted different particle concentration in fluids. These figures showed no chaining phenomenon of particles



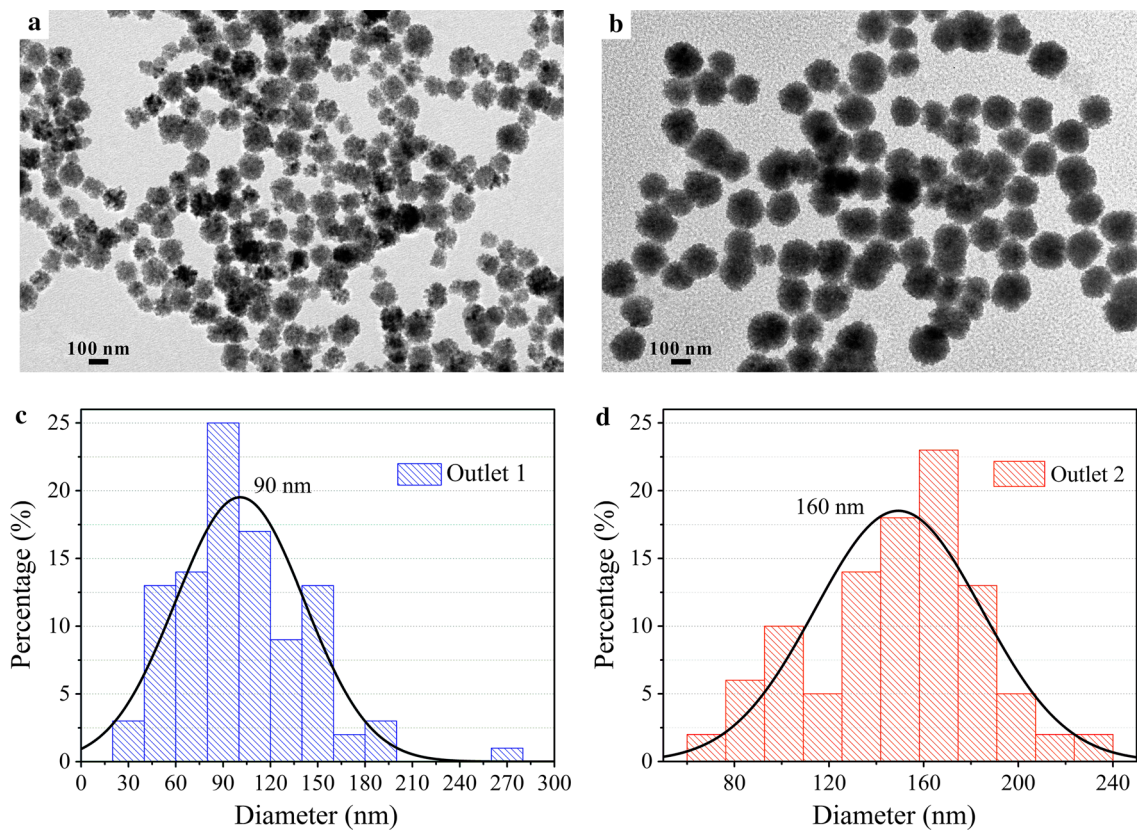


Fig. 10 TEM images of the obtained Fe₃O₄ nanospheres in outlet 1 of (a), outlet 2 of (b). Histograms of particles sizes distribution of the obtained Fe₃O₄ nanospheres in outlet 1 of (c) 90 nm, outlet 2 of (d) 160 nm through dynamic light scattering

The two fluids possessed a significant mean diameter difference. The transmission electron microscopy (TEM) images were obtained by a JEM-2100F at an accelerating voltage of 200 kV. Dynamic light scattering (DLS) was also conducted by a Zetasizer Nano (Malvern Corp.) to depict the particle size distribution of the obtained the two fluid samples. All of these results are shown in Fig. 10. In (a) and (c), the smaller size range was apparent as observed in the micrograph and histogram. In (b) and (d), the larger sizes were successfully recovered after separation. Both the TEM images and histograms of DLS showed the difference in particle sizes at two exits. It was found that the average diameters of outlet 1 and outlet 2 were 90 and 160 nm, respectively. These testing results proved the validity of the experimental manipulation. The results of numerical simulation were used to illustrate the effectiveness of our method, and the conclusion of numerical simulation was also proved by the experimental results.

Due to the accuracy of this experimental setup, a certain range of particle size coincidence occurred. In addition, numerical simulation results also showed there would be a certain particle size coincidence (Figs. 6c–h and 8). There was a significant reduction in the particle size width of the nanospheres before and after separation. We intend

to consider the influent parameters such as inlet flow rates and channel geometry in the next work to study the separation efficiency. Besides, our present work focused on the convenience of the experimental setup and the placement of suitable magnet by numerical simulations.

Although there are several methods to prepare monodispersed nanospheres, most of the present approaches only produced polydispersed magnetic particles with broad distribution. Our ideal will improve the efficiency for monodispersed magnetic particles because of the easy processing.

5 Conclusions

We developed the sorting manipulation of magnetic nanospheres using a microfluidic channel equipped with a single permanent magnet. The polydisperse Fe₃O₄ nanospheres with a broad sizes (from 40 to 280 nm) distribution could be separated into two fluids with a significant difference in average diameters. After the magnetic separation, the width of the particle size range was reduced significantly. The particle size of outlet 1 was mainly concentrated in the 60 to 150 nm, while the outlet 2 was 120–200 nm. There was a

significant reduction in the particle size range of the nanospheres before and after separation. We identified this as a successful separation.

Because of the low Reynolds number of microfluidic flow, inertial effect on the nanospheres is negligible and then the migrations are attributed to Stokes drag force and magnetophoresis force. In addition, numerical simulations were used to predict and optimize the particles trajectories in the channel. The magnetic flux density and magnetic field gradient along the main path of the channel when the permanent magnet was placed at different positions were calculated. The thresholds of particles diameters obtained in simulations were diverse at each position of permanent magnet in a constant inlet flow rate. Furthermore, we showed particles' trajectories in both simulations results and experimental photographic pictures. Finally, synthesizing real-time images of the microfluidic channel through a CCD camera and thresholds versus magnet positions helped us to find the most suitable position of the permanent magnet conveniently.

Acknowledgements Financial support from the National Natural Science Foundation of China (Grant Nos. 11572309, 11572310), the Strategic Priority Program of the Chinese Academy of Science (Grant No. XDB2204502) and the Fundamental Research Funds for the Central Universities (WK248000002) are gratefully acknowledged. This work was also supported by Collaborative Innovation Center of Suzhou Nano Science and Technology.

References

- Bao G, Mitragotri S, Tong S (2013) Multifunctional nanoparticles for drug delivery and molecular imaging. *Annu Rev Biomed Eng* 15:253–282
- Carpino F, Zborowski M, Williams PS (2007) Quadrupole magnetic field-flow fractionation: a novel technique for the characterization of magnetic nanoparticles. *J Magn Magn Mater* 311:383–387
- Chatterjee J, Haik Y, Chen C-J (2003) Size dependent magnetic properties of iron oxide nanoparticles. *J Magn Magn Mater* 257:113–118
- Cheng R, Zhu T, Mao L (2014) Three-dimensional and analytical modeling of microfluidic particle transport in magnetic fluids. *Microfluid Nanofluid* 16:1143–1154
- Choi HS, Liu W, Misra P, Tanaka E, Zimmer JP, Ipe BI, Bawendi MG, Frangioni JV (2007) Renal clearance of quantum dots. *Nat Biotechnol* 25:1165–1170
- Duffy DC, McDonald JC, Schueller OJ, Whitesides GM (1998) Rapid prototyping of microfluidic systems in poly (dimethylsiloxane). *Anal Chem* 70:4974–4984
- Fang Q, Xuan S, Jiang W, Gong X (2011) Yolk-like micro/nanoparticles with superparamagnetic iron oxide cores and hierarchical nickel silicate shells. *Adv Funct Mater* 21:1902–1909
- Figuerola A, Fiore A, Di Corato R, Falqui A, Giannini C, Micotti E, Lascialfari A, Corti M, Cingolani R, Pellegrino T (2008) One-pot synthesis and characterization of size-controlled bimagnetic FePt-iron oxide heterodimer nanocrystals. *J Am Chem Soc* 130:1477–1487
- Furlani E (2006) Analysis of particle transport in a magnetophoretic microsystem. *J Appl Phys* 99:024912
- Gijs MA, Lacharme F, Lehmann U (2009) Microfluidic applications of magnetic particles for biological analysis and catalysis. *Chem Rev* 110:1518–1563
- Groisman A, Quake SR (2004) A microfluidic rectifier: anisotropic flow resistance at low Reynolds numbers. *Phys Rev Lett* 92:094501
- Han X, Feng Y, Cao Q, Li L (2014) Three-dimensional analysis and enhancement of continuous magnetic separation of particles in microfluidics. *Microfluid Nanofluid* 18:1209–1220
- Hejazian M, Nguyen N-T (2015) Negative magnetophoresis in diluted ferrofluid flow. *Lab Chip* 15:2998–3005
- Hejazian M, Li W, Nguyen N-T (2015) Lab on a chip for continuous-flow magnetic cell separation. *Lab Chip* 15:959–970
- Hejazian M, Nguyen N-T (2016) Magneto-fluidic concentration and separation of non-magnetic particles using two magnet arrays. *Biomicrofluidics* 10:044103
- Hejazian M, Phan D-T, Nguyen N-T (2016) Mass transport improvement in microscale using diluted ferrofluid and a non-uniform magnetic field. *RSC Adv* 6:62439–62444
- Iiguni Y, Suwa M, Watarai H (2004) High-magnetic-field electro-magnetophoresis of micro-particles in a capillary flow system. *J Chromatogr A* 1032:165–171
- Kim H-J, Phenrat T, Tilton RD, Lowry GV (2009) Fe₀ nanoparticles remain mobile in porous media after aging due to slow desorption of polymeric surface modifiers. *Environ Sci Technol* 43:3824–3830
- Latham AH, Freitas RS, Schiffer P, Williams ME (2005) Capillary magnetic field flow fractionation and analysis of magnetic nanoparticles. *Anal Chem* 77:5055–5062
- Lee H, Xu L, Ahn B, Lee K, Oh KW (2012) Continuous-flow in-droplet magnetic particle separation in a droplet-based microfluidic platform. *Microfluid Nanofluid* 13:613–623
- Liu S, Lu F, Jia X, Cheng F, Jiang LP, Zhu JJ (2011) Microwave-assisted synthesis of a biocompatible polyacid-conjugated Fe₃O₄ superparamagnetic hybrid. *CrystEngComm* 13:2425–2429
- Munir A, Wang J, Li Z, Zhou HS (2009a) Numerical analysis of a magnetic nanoparticle-enhanced microfluidic surface-based bioassay. *Microfluid Nanofluid* 8:641–652
- Munir A, Wang J, Zhou HS (2009b) Dynamics of capturing process of multiple magnetic nanoparticles in a flow through microfluidic bioseparation system. *IET Nanobiotechnol* 3:55–64
- Munir A, Wang J, Zhu Z, Zhou HS (2010) Residence time distribution analysis of magnetic nanoparticle-enhanced mixing using time-dependent magnetic actuation in microfluidic system. *Microfluid Nanofluid* 10:735–747
- Munir A, Wang J, Zhu Z, Zhou HS (2011) Mathematical modeling and analysis of a magnetic nanoparticle-enhanced mixing in a microfluidic system using time-dependent magnetic field. *IEEE T Nanotechnol* 10:953–961
- Munir A, Zhu Z, Wang J, Zhou HS (2014) Experimental investigation of magnetically actuated separation using tangential microfluidic channels and magnetic nanoparticles. *IET Nanobiotechnol* 8:102–110
- Phan NT, Jones CW (2006) Highly accessible catalytic sites on recyclable organosilane-functionalized magnetic nanoparticles: An alternative to functionalized porous silica catalysts. *J Mol Catal A: Chem* 253:123–131
- Rodriguez-Villarreal AI, Tarn MD, Madden LA, Lutz JB, Greenman J, Samitier J, Pamme N (2011) Flow focussing of particles and cells based on their intrinsic properties using a simple diamagnetic repulsion setup. *Lab Chip* 11:1240–1248

- Shen F, Hwang H, Hahn YK, Park JK (2012) Label-free cell separation using a tunable magnetophoretic repulsion force. *Anal Chem* 84:3075–3081
- Singh A, Sahoo SK (2014) Magnetic nanoparticles: a novel platform for cancer theranostics. *Drug Discov Today* 19:474–481
- Song X, Luo X, Zhang Q, Zhu A, Ji L, Yan C (2015) Preparation and characterization of biofunctionalized chitosan/Fe₃O₄ magnetic nanoparticles for application in liver magnetic resonance imaging. *J Magn Magn Mater* 388:116–122
- Stephens JR, Beveridge JS, Williams ME (2012) Analytical methods for separating and isolating magnetic nanoparticles. *PCCP* 14:3280–3289
- Tzirtzilakis E (2005) A mathematical model for blood flow in magnetic field. *Phys Fluids* 17:077103
- Veisheh O, Gunn JW, Zhang M (2010) Design and fabrication of magnetic nanoparticles for targeted drug delivery and imaging. *Adv Drug Deliv Rev* 62:284–304
- Vilkner T, Janasek D, Manz A (2004) Micro total analysis systems. Recent developments. *Anal Chem* 76:3373–3386
- Whitesides GM (2006) The origins and the future of microfluidics. *Nature* 442:368–373
- Xi Z, Huang R, Li Z, He N, Wang T, Su E, Deng Y (2015) Selection of HBsAg-specific DNA aptamers based on carboxylated magnetic nanoparticles and their application in the rapid and simple detection of hepatitis B virus infection. *ACS Appl Mat Inter* 7:11215–11223
- Xuan S, Wang F, Wang Y-XJ, Jimmy CY, Leung KC-F (2010) Facile synthesis of size-controllable monodispersed ferrite nanospheres. *J Mater Chem* 20:5086–5094
- Yavuz CT, Mayo J, William WY, Prakash A, Falkner JC, Yean S, Cong L, Shipley HJ, Kan A, Tomson M (2006) Low-field magnetic separation of monodisperse Fe₃O₄ nanocrystals. *Science* 314:964–967
- Zeng J, Chen C, Vedantam P, Tzeng T-R, Xuan X (2012) Magnetic concentration of particles and cells in ferrofluid flow through a straight microchannel using attracting magnets. *Microfluid Nanofluid* 15:49–55
- Zhou Y, Kumar DT, Lu X, Kale A, DuBose J, Song Y, Wang J, Li D, Xuan X (2015) Simultaneous diamagnetic and magnetic particle trapping in ferrofluid microflows via a single permanent magnet. *Biomicrofluidics* 9:044102
- Zhu T, Marrero F, Mao L (2010) Continuous separation of non-magnetic particles inside ferrofluids. *Microfluid Nanofluid* 9:1003–1009
- Zhu J, Liang L, Xuan X (2011) On-chip manipulation of nonmagnetic particles in paramagnetic solutions using embedded permanent magnets. *Microfluid Nanofluid* 12:65–73
- Zhu T, Cheng R, Lee SA, Rajaraman E, Eiteman MA, Querec TD, Unger ER, Mao L (2012) Continuous-flow ferrohydrodynamic sorting of particles and cells in microfluidic devices. *Microfluid Nanofluid* 13:645–654